Physica D ▮ (▮▮▮▮) ▮▮▮–▮▮▮

Contents lists available at SciVerse ScienceDirect

Physica D

journal homepage: www.elsevier.com/locate/physd

Turbulent mixing of clouds with the environment: Small scale two phase evaporating flow investigated in a laboratory by particle image velocimetry

Piotr M. Korczyk [a,b], Tomasz A. Kowalewski [a], Szymon P. Malinowski [c,*]

[a] Institute of Fundamental Technological Research, Polish Academy of Sciences, Pawinskiego 5B, 02-106 Warsaw, Poland
[b] Institute of Physical Chemistry, Polish Academy of Sciences, Kasprzaka 44/52, 01-224 Warsaw, Poland
[c] Institute of Geophysics, Faculty of Physics, University of Warsaw, Pasteura 7, 02-093 Warsaw, Poland

ARTICLE INFO

Article history:
Available online xxxx

Keywords:
Small-scale turbulence
Atmospheric turbulence
Evaporative cooling
Cloud-clear-air mixing

ABSTRACT

In this report, experiments mimicking some aspects of cloud-clear-air mixing in a laboratory chamber are discussed. A saturated plume containing small droplets of water (a surrogate of an atmospheric cloud) is mixed with unsaturated environmental air in order to study effect of evaporative cooling at the interfaces between cloudy and clear air filaments on small-scale turbulence. Two components of the turbulent velocity at a small scale are determined using particle imaging velocimetry of the cloud droplets. Enhanced velocity fluctuations between the Kolmogorov ($\eta \approx 0.8$ mm) and Taylor ($\lambda \approx 8$ mm) microscales are observed.

The characteristic feature of these microscales is anisotropy with a preferred vertical direction. A straightforward dependence of the observed effects on the relative humidity of the environment indicates the importance of buoyancy production by evaporative cooling. This conclusion is in agreement with previous numerical experiments described in the literature and suggests that, under certain conditions, effects similar to the above may influence the smallest scales of turbulence in natural clouds.

1. Introduction

Measurements of the smallest scales of turbulence and the turbulent mixing of passive scalars performed in controlled laboratory conditions have been widely documented in the scientific literature (reviewed in [1–3]). In contrast, experimental evidence of the smallest scales of natural atmospheric turbulence is limited ([4] and the references therein). By "smallest-scale" we are referring here to turbulence at the edge of the inertial range, i.e., at scales from approximately 10 cm (the practical resolution limit of high-resolution airborne instruments) to the Kolmogorov microscale, η (which, for typical atmospheric flows, is of the order of 1 mm).

Clouds are an atmospheric phenomenon in which turbulence plays an important role. Through nonlinear interactions, cloud turbulence influences all scales of motion: from droplet collisions to global-scale circulation [5,6]. Cloud turbulence occurs over a range of scales extending further than in laboratory flows, from hundreds of meters down to a fraction of a millimeter. The typical Reynolds numbers, *Re*, can reach 10^9 and Taylor microscale Reynolds number may be as high as $Re_\lambda \sim 10^5$. However, the mean turbulent kinetic energy (*TKE*) dissipation rate ε is typically low in clouds, relative to typical laboratory experiments, ranging from $\varepsilon = 10^{-1}$ m^2 s^{-3} to $\varepsilon = 10^{-5}$ m^2 s^{-3} in stratiform and shallow cumulus clouds, and these values are highly variable at distances of hundreds of meters [7].

Investigations of turbulence in the atmosphere are different from those in the lab. In the lab, we control the external parameters of turbulence, whereas in the atmosphere, we make observations but can often miss many important parameters. In the lab, we know (almost) everything about the source of *TKE*. We can force the turbulence to be stationary, measure its uniformity, or try to make it isotropic. When performing measurements in the free atmosphere, we often have only a crude idea of the *TKE* sources, such as shear instability, gravity wave breaking, dry or moist convection driven by latent heat changes or radiative effects. Clouds (especially convective ones) have various life cycles; some regions are more turbulent than others. Turbulence can be transported by advection, and transport terms in the turbulent kinetic energy equation usually cannot be neglected. Point in-situ measurements often do not reveal the whole complexity and scale dependence of the flow.

Laboratory investigations of turbulence can help explain specific aspects of this natural phenomenon. Experiments in controlled, or at least closely monitored, conditions give a good insight into the details of phenomena that are not available in situ. Even when extensions of laboratory studies to the real world

* Corresponding author. Tel.: +48 22 55 46 860; fax: +48 22 55 46 882.
E-mail address: malina@fuw.edu.pl (S.P. Malinowski).

0167-2789/$ – see front matter © 2011 Elsevier B.V. All rights reserved.
doi:10.1016/j.physd.2011.11.003

are not straightforward, they help to build an understanding of free atmospheric flows. This study is an example of such research: we describe a laboratory experiment aimed at representing some features of small-scale turbulence that we cannot observe outdoors using the existing experimental techniques. The laboratory set-up differs substantially from what occurs in clouds; nevertheless, it allows us to focus on *TKE* production due to the buoyancy forces resulting from evaporative cooling of cloud droplets in the course of cloud-clear-air mixing.

Let us consider isobaric mixing between two parcels of air at similar temperatures: one cloudy, i.e., saturated, containing condensed water, and a second one unsaturated, without cloud droplets. In the course of mixing, a certain amount of liquid water evaporates, cooling the mixture and consequently reducing its buoyancy (increasing its density). The final effect depends on the initial temperature of both of the parcels, the humidity of dry parcel, the liquid water content (*LWC*) of the wet parcel and the proportion of masses in the mixing event. It is well documented in the meteorological literature that such processes reduce cloud growth [8], and drive formation of downdrafts around clouds (e.g. [9,10]). Paluch [11] introduced diagrams illustrating buoyancy reduction for varying mixing proportion (cf. Figs. 9–11 therein). Deardorff [12] and Randall [13] found that on the top of stratiform cloud mixing and subsequent evaporative cooling may lead to destabilization of cloud layer (cloud top mixing instability). Recent direct numerical simulations by Mellado [14,15] show details of such process. Formulation of moist cloud processes by Pauluis and Schumacher [16] elegantly represent the buoyancy effects of a phase change in atmospheric simulations.

Although thermodynamics and bulk dynamics of cloud-clear-air mixing have been widely investigated, the corresponding microphysical aspects have received much less attention. The authors of [17] proposed to study the small-scale effects of cloud-clear-air mixing inside a laboratory chamber. High-resolution numerical simulations aimed at interpreting their measurements were carried out in [18–20]. An improved version of the chamber experiment was reported in [21], and the results of the laboratory and numerical experiments were compared in [22].

This paper extends the preliminary experimental results of [21] to a wide range of relative humidities. Improvements in the experimental technique allow us to observe the evolution of mixing and to analyze the structure functions and autocorrelations of the velocity fluctuations. Additionally, the present work includes experiments with non-evaporating droplets that were performed to distinguish between the small-scale effects of buoyancy fluctuations due to mass loading and those due to evaporative cooling.

2. Experimental set-up

2.1. Cloud chamber and imaging technique

The experimental set-up evolved from the earlier studies described in [17,21]. The aim of the set-up design was to use a particle imaging velocimetry (PIV) technique [23] to examine the motion of cloud droplets in a cloudy plume undergoing mixing with an unsaturated environment. The cloud (cloud droplets) was generated by a commercial ultrasonic humidifier. The size spectrum of the droplets was verified using a well-known technique: sedimenting droplets were collected on a glass plate covered with an oil film to prevent evaporation. Microscopic photographs of the droplets in oil (Fig. 1) were processed using a custom-designed pattern recognition algorithm for detecting droplet sizes. The observed mean droplet radius $R_m \approx 5.4\ \mu$m corresponds well to reported observational data, and the spectral width of the droplet size spectrum (standard deviation of radius 1.6 μm) is only slightly wider than the typical value for clouds [24].

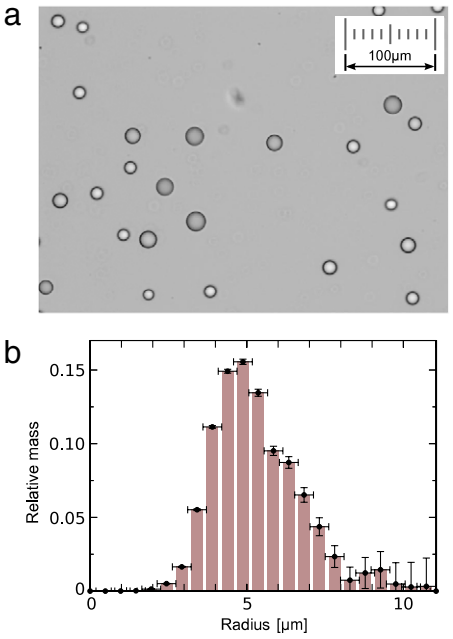

Fig. 1. (a) Sample image of droplets collected in a film of silicone oil, observed with a microscope. (b) Measured initial droplet spectrum. Vertical axis: relative mass; horizontal axis: droplet radius (μm).

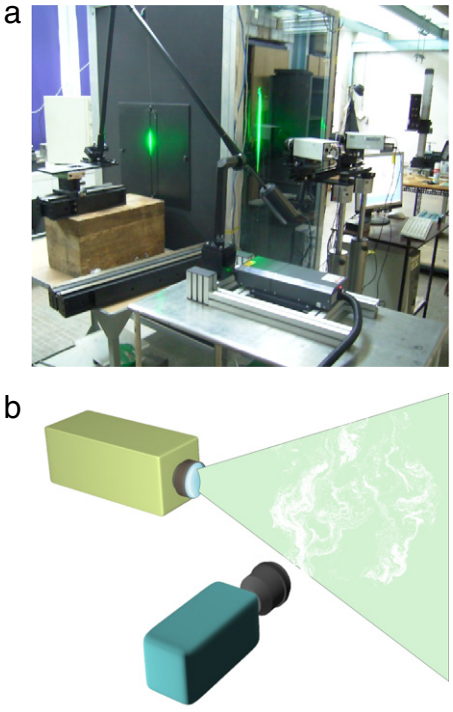

Fig. 2. (a) Cloud chamber (black box with aluminum frame) with a laser and optical system producing a planar sheet of light and CCD cameras (here, configured for stereo PIV, not presented in the paper). (b) Principle of the visualization technique. A pulsed laser with a suitable optical system produces a planar sheet of light. The light scattered by the cloud droplets is imaged by a CCD camera with its optical axis normal to the light sheet.

The experimental apparatus and an illustration of the measurement system are shown in Fig. 2. The core is a glass-walled cloud chamber of dimensions: 1 m × 1 m × 1.8 m, in which a turbulent plume was produced. The cloud (a saturated airmass with a load of droplets) was buffered in a box above the main chamber. When the box is filled, a round hole (of diameter 10 cm) between the box

Please cite this article in press as: P.M. Korczyk, et al., Turbulent mixing of clouds with the environment: Small scale two phase evaporating flow investigated in a laboratory by particle image velocimetry, Physica D (2011), doi:10.1016/j.physd.2011.11.003

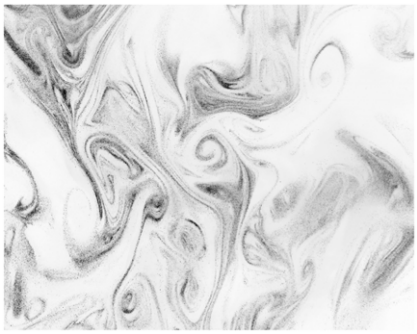

Fig. 3. An image from the experimental chamber showing small-scale structures created in the process of cloud-clear-air mixing. The imaged area corresponds to an 8×6 cm^2 in physical region.

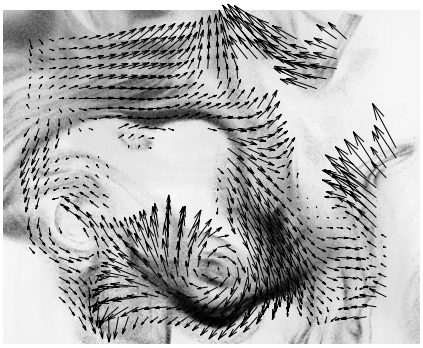

Fig. 4. Two components of the velocity field retrieved with a PIV technique for cloudy filaments.

and the chamber opens and the cloud descends as a saturated, negatively buoyant turbulent plume that mixes with the unsaturated air in the chamber. This mixing was imaged using a light sheet technique. Two lasers (Nd:Yag, wavelength 532 nm, pulse energy 36 mJ, pulse length 5ns) were used to produce pairs of flashes at a rate of 12 Hz. Light, shaped by cylindrical lenses, provides a 1-mm-thick sheet of about 15 cm width in the region of interest. The light scattered by the droplets was imaged with high resolution CCD cameras (PCO Sensi-Cam) in conjunction with a frame grabber and a recording PC computer. Pairs of 1280×1024 pixels 12 bit images were stored in the computer's RAM. A sample image from the experiment, covering an area of $\sim 8 \times 6$ cm^2, is presented in Fig. 3. It reveals a fine structure created in the course of turbulent mixing between the cloud and the unsaturated environment. One pixel in the image corresponds to a 1.2-mm-deep volume with a $\sim 69 \times 69$ μm^2 area in the plane of the laser-light sheet. Such elementary volumes occupied by the droplets are represented by dark pixels; bright pixels correspond to the volumes that are void of droplets.

Pattern recognition using a pair of images separated by a known time interval allows us to retrieve two velocity components in the image plane. Clear air filaments do not contain markers; thus, velocity retrieval is limited to cloud filaments only: a cloud mask is adopted in PIV algorithms to remove possible spurious vectors in the clear areas. Two original, accurate multi-scale PIV algorithms were developed for this experiment [25]. These algorithms allow us to estimate the two velocity components of the droplets carried by the flow with a spatial resolution of $\sim$0.07 mm; i.e., an order of magnitude smaller than the Kolmogorov length scale (estimated as $\eta = 0.76$ mm for the measurements). Fig. 4 shows a sample pattern of droplets superimposed on the retrieved vectors of velocity fluctuations (with the mean velocity within the image area removed).

Here, we note several properties specific to this experiment. We are not employing particle tracking to investigate the Lagrangian behavior of inertial particles in the flow [26], nor do we use typical PIV in which the flow is seeded with passive markers. The droplets have non-negligible inertia and actively interact with the flow through mass loading, evaporative cooling, gravity, and Stokes interaction. While the last two effects are small and should not have a significant effect on the turbulence (the Stokes number with respect to the turbulence accelerations is 0.003 and the Stokes time for adjusting to the acceleration of gravity is $\sim 10^{-3}$ s), the first two effects may substantially impact the flow, presumably in a manner that is similar to real atmospheric clouds.

The plume descending through the central part of the chamber forces airflow recirculation inside the chamber. The imaging is restricted to the central part of the chamber to avoid regions of shear in the chamber-scale circulation. Turbulence resulting from this shear can be considered as a surrogate of turbulence produced by larger-scale circulation in natural clouds.

2.2. Measurements

The initial velocity of the plume at the inlet to the chamber, as estimated from 300 pairs of images is $\sim$17 cm/s. Initially, the flow is not laminar, and the analysis of the velocity field using the proper orthogonal decomposition (POD) technique indicates that its first mode contains about 28% of the kinetic energy of the flow, whereas the second mode contains about 12%, with a series of modes with consecutively decreasing energies. The inflow is symmetrical with respect to the plume axis, and at least the first six modes show patterns that are nearly symmetric. The descending plume strongly mixes with the unsaturated air inside the chamber, creating complicated, continuously evolving filaments. The retrieval of velocity fluctuations within the cloudy filaments gives insight into the mixing details.

The initial mass loading (liquid water content, *LWC*) in the plume reaches $\sim$23.7 g/kg (0.0237 in SI units), which is an order of magnitude more than that observed in natural clouds. This value was measured by a weight method in which a given volume of cloud is sucked through a cotton swab filter. The difference in the weight of the cotton filter before and after sucking allows us to estimate the mass of collected water. The temperature of the plume measured at the inlet was about 25 °C, close to the temperature of the unsaturated air in the chamber. The temperature inside the chamber was monitored by a vertical chain of ten thermocouple sensors. The relative humidity (*RH*) of the air inside the chamber was monitored by an analogous chain of four capacity hygrometers. The initial *RH* inside the chamber was, in some series, as low as 20% and increased to 65% during the course of the experiments.

In each measurement lasting about 30 s a sequence of 100 pairs of images covering an area of 8×6 cm^2 is captured. Short duration of the experimental series allows us to assume constant properties of the environment during the series. A time lapse of approximately 0.3 s between the pairs of images ensures that consecutive scenes are independent, as the mean downward velocity of the plume is $\sim$20 cm/s. Velocity fluctuations (with the mean velocity subtracted) were collected for 100 independent scenes under consistent conditions, providing information on the statistical properties of the flow. The measurements were performed at various distances from the inlet (30–70 cm) to include various stages of mixing. The thermodynamic conditions were monitored and recorded during the measurements. This factor is important because the thermodynamics, especially the *RH* of the environmental air, influence the droplet evaporation. After the measurement, the chamber was opened, ventilated and cleaned to be prepared for the new series. The results from 50 series of measurements are summarized in Table 1.

Please cite this article in press as: P.M. Korczyk, et al., Turbulent mixing of clouds with the environment: Small scale two phase evaporating flow investigated in a laboratory by particle image velocimetry, Physica D (2011), doi:10.1016/j.physd.2011.11.003

Table 1
Results from 50 experimental series with evaporating droplets. Pos.—position of measurement (distance from the top of the chamber); *RH*—relative humidity; ε—*TKE* dissipation rate; η—Kolmogorov length; $\langle\rangle$—averaging; u and w—horizontal and vertical component of velocity; σ standard deviation; S—skewness; K—kurtosis; λ—Taylor microscale.

No.	Pos. [cm]	*RH* [%]	ε [m^2 s^{-3}]	η [mm]	$\langle u\rangle$[m s^{-1}]	$\langle w\rangle$[m s^{-1}]	σ_u[m s^{-1}]	σ_w[m s^{-1}]	$S(u)$	$S(w)$	$K(u)$	$K(w)$	λ_u[mm]	λ_w[mm]
1	70	20	0.016	0.68	−0.002	0.30	0.050	0.062	−0.04	0.03	3.0	2.8	5.4	6.6
2	70	42	0.007	0.84	0.009	0.26	0.042	0.052	−0.09	0.09	3.0	2.8	7.4	9.3
3	70	49	0.006	0.88	0.009	0.24	0.044	0.052	−0.08	0.01	2.9	2.8	8.9	11.0
4	70	61	0.006	0.89	0.013	0.23	0.038	0.052	−0.03	0.01	3.0	2.9	8.0	1.2
5	60	25	0.011	0.75	−0.015	0.28	0.048	0.059	−0.02	0.07	2.9	2.7	6.2	7.8
6	60	20	0.012	0.73	0.001	0.30	0.049	0.056	−0.10	0.01	2.9	2.9	6.0	7.0
7	60	29	0.010	0.77	−0.007	0.27	0.045	0.056	0.03	0.11	2.8	2.6	6.4	7.8
8	60	40	0.009	0.79	−0.001	0.28	0.046	0.054	−0.06	−0.05	3.3	2.8	6.8	8.1
9	60	62	0.005	0.90	0.004	0.21	0.039	0.047	−0.06	−0.02	2.9	2.8	8.8	11.0
10	50	62	0.007	0.84	0.008	0.24	0.042	0.055	−0.08	0.00	2.9	2.7	7.5	10.0
11	50	25	0.014	0.71	0.013	0.22	0.042	0.057	0.01	0.00	2.9	2.9	7.0	6.7
12	50	32	0.012	0.73	0.002	0.27	0.046	0.064	−0.07	0.06	3.2	2.8	5.8	7.8
13	50	42	0.010	0.77	0.001	0.25	0.047	0.062	0.01	−0.04	2.8	2.6	6.5	8.9
14	50	50	0.007	0.85	−0.001	0.21	0.038	0.054	−0.11	0.17	3.1	3.0	7.2	9.7
15	50	61	0.008	0.81	0.003	0.22	0.045	0.056	−0.12	−0.05	2.9	2.7	7.2	9.3
16	40	59	0.009	0.79	0.014	0.22	0.045	0.062	−0.18	0.10	3.2	2.5	6.7	9.2
17	40	20	0.014	0.71	0.002	0.27	0.050	0.064	0.04	−0.14	2.7	2.7	5.4	6.9
18	40	32	0.012	0.73	0.000	0.24	0.044	0.062	−0.07	0.02	3.0	2.9	5.6	7.6
19	40	41	0.011	0.75	0.002	0.25	0.046	0.062	−0.07	0.00	3.0	2.7	5.9	7.8
20	40	52	0.010	0.77	0.016	0.24	0.044	0.063	0.06	0.06	2.9	2.7	6.0	9.0
21	40	46	0.011	0.75	0.006	0.24	0.046	0.057	−0.08	0.03	2.9	2.7	6.0	7.4
22	40	48	0.008	0.80	0.010	0.21	0.040	0.056	−0.09	0.15	2.9	2.8	6.0	8.2
23	30	56	0.011	0.75	0.011	0.16	0.043	0.062	−0.06	0.03	3.0	2.7	5.5	7.7
24	30	65	0.007	0.83	0.013	0.18	0.037	0.050	−0.01	0.15	3.0	3.0	6.4	8.3
25	30	20	0.021	0.64	−0.001	0.21	0.053	0.064	−0.07	−0.13	2.9	2.9	4.6	5.5
26	30	36	0.017	0.67	−0.011	0.18	0.044	0.057	−0.08	0.04	3.3	2.8	4.3	5.5
27	30	23	0.021	0.64	0.002	0.19	0.052	0.067	−0.02	−0.16	3.0	2.9	4.6	6.0
28	50	23	0.014	0.70	0.006	0.23	0.052	0.061	0.04	−0.27	3.1	2.8	4.3	4.9
29	70	23	0.016	0.69	0.005	0.27	0.050	0.060	−0.04	0.00	2.9	2.8	4.5	5.4
30	70	23	0.015	0.69	0.008	0.25	0.048	0.058	−0.10	0.13	3.2	3.1	5.2	6.1
31	70	23	0.014	0.71	0.013	0.25	0.046	0.052	−0.01	0.02	3.1	2.9	5.7	6.3
32	70	23	0.014	0.70	−0.002	0.25	0.047	0.054	−0.11	0.14	3.3	3.2	4.8	5.6
33	70	23	0.015	0.69	0.008	0.26	0.049	0.060	−0.08	0.13	3.1	3.1	5.2	6.1
34	70	23	0.014	0.71	0.000	0.26	0.046	0.053	0.06	0.03	3.0	2.8	5.6	6.4
35	70	38	0.008	0.82	0.012	0.24	0.043	0.059	−0.11	0.07	3.0	2.8	7.3	10.0
36	50	46	0.007	0.83	0.010	0.20	0.040	0.058	−0.11	0.08	3.0	2.9	7.1	10.0
37	50	23	0.014	0.70	0.004	0.24	0.049	0.063	−0.06	−0.02	2.9	2.9	5.4	7.1
38	50	29	0.009	0.79	0.007	0.20	0.040	0.055	−0.16	0.04	2.8	2.9	6.3	8.5
39	50	24	0.013	0.71	−0.023	0.23	0.049	0.058	−0.07	0.10	3.2	3.1	5.4	6.4
40	50	33	0.008	0.80	−0.008	0.21	0.041	0.051	−0.07	0.17	3.0	3.0	6.6	8.0
41	50	24	0.013	0.72	−0.005	0.23	0.047	0.065	−0.13	0.19	2.9	2.7	5.6	7.3
42	30	21	0.023	0.63	0.011	0.19	0.050	0.066	−0.01	−0.02	3.0	2.7	4.2	5.4
43	30	21	0.023	0.62	0.012	0.18	0.052	0.069	−0.04	−0.02	3.1	2.7	4.4	5.8
44	30	21	0.023	0.62	0.013	0.19	0.050	0.070	−0.09	0.01	3.1	2.6	4.1	5.7
45	30	21	0.023	0.63	−0.006	0.17	0.050	0.065	−0.10	0.08	3.1	2.7	4.3	5.6
46	30	32	0.018	0.66	0.014	0.19	0.047	0.070	−0.06	0.06	3.1	2.8	4.3	6.6
47	30	42	0.016	0.68	0.014	0.18	0.042	0.064	−0.06	0.00	3.2	2.8	4.1	6.2
48	30	46	0.013	0.72	−0.006	0.17	0.045	0.061	−0.17	0.11	3.1	2.8	5.1	6.8
49	30	51	0.011	0.75	0.011	0.16	0.041	0.065	−0.18	0.18	3.2	2.9	5.1	7.8
50	30	31	0.015	0.69	0.018	0.13	0.040	0.066	−0.07	0.20	3.3	2.8	4.2	6.6

3. Results

3.1. Effects of evaporative cooling on buoyancy

To analyze the role of evaporative cooling of water droplets at the cloud-clear air interface on the buoyancy fluctuations, we consider so called density temperature T_ρ of cloudy air [27, Eq. 4.3.6] defined as

$$T_\rho \approx T\left(1+\left(1-\frac{R_v}{R_a}\right)X - LWC\right), \tag{1}$$

where T denotes temperature, X is the water vapor mixing ratio (the mass of water vapor divided by the mass of dry air), *LWC* is the liquid water mixing ratio (the mass of water droplets divided by the mass of dry air), R_a and R_v are the gas constants of dry air and water vapor, respectively. These values are determined by $R_a = R/\mu_a$, $R_v = R/\mu_v$, where R is the universal gas constant and μ_a, μ_v are the molar masses of dry air and water respectively. T_ρ is inversely proportional to the mean density.

Let us consider the density temperature of a homogeneous mixture of cloudy air and an unsaturated environmental air at a given mixing proportion χ (where χ is the ratio of the mass of the cloudy air to the sum of the masses of both kinds of air, [28,19]). The assumption that the portions of air are in thermodynamic equilibrium before and after mixing implies that some of the droplets evaporate during the course of mixing. The dependence of the density temperature T_ρ on the proportion of mixing χ for initial conditions corresponding to the conditions in the chamber (*LWC* of cloudy air 23.7 g/kg, temperature of both portions 25 °C) is shown in Fig. 5.

The interpretation of Fig. 5 is the following: $\chi = 1$ indicates the T_ρ of the cloud calculated with the Eq. (1) and $\chi = 0$ indicates T_ρ of the environment for various *RH*. Without phase change effects the density temperature of the mixture would lay on a straight segments connecting T_ρ of the cloud and T_ρ of the environment. Evaporation of water substance reduces T_ρ of the uniform, homogenized mixture consisting of mass fraction χ of the cloud and 1-χ of the environment. In the experimental conditions

Please cite this article in press as: P.M. Korczyk, et al., Turbulent mixing of clouds with the environment: Small scale two phase evaporating flow investigated in a laboratory by particle image velocimetry, Physica D (2011), doi:10.1016/j.physd.2011.11.003

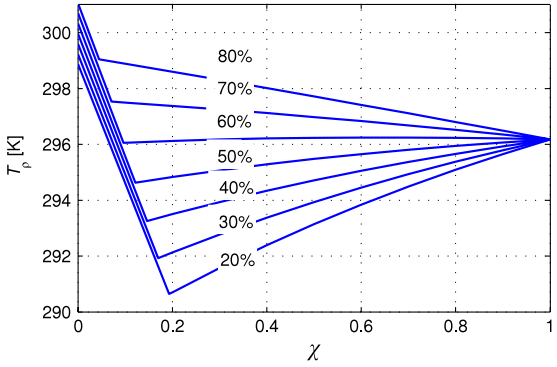

Fig. 5. Mixing diagrams (vertical axis: density temperature, horizontal axis: mixing proportion of cloudy air) for conditions in the cloud chamber, as calculated by a simple model assuming thermodynamic equilibrium before and after mixing.

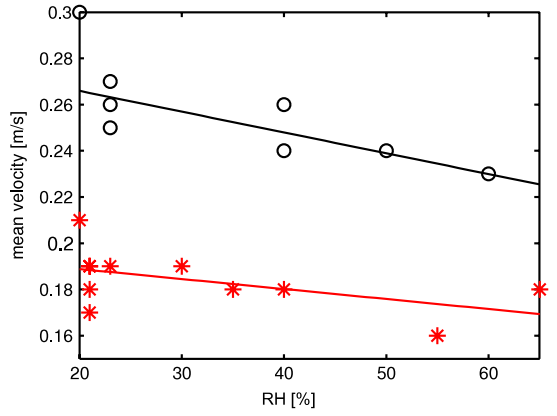

Fig. 6. Mean downward velocity of the plume at 30 cm (black, circles) and 70 cm (red, stars) from the inlet as a function of the relative humidity (*RH*) of the environmental air. The lines represent best the linear fits. (For interpretation of the references to colour in this figure legend, the reader is referred to the web version of this article.)

the mixing of the cloud with the unsaturated environment of *RH* less than ∼60% may result in a mixture that is denser than either component. The minimum density temperature is obtained for mixtures containing ∼80% of cloudy air and ∼20% of unsaturated environment.

Assuming varying proportions χ of cloud and clear air in various mixed volumes, a wide distribution of T_ρ and, consequently, a remarkable small-scale variability of the buoyancy field result from mixing. A detailed analysis of the buoyancy fluctuations can be found in Sections 2 and 3 of [22].

3.2. Bulk plume motion

In the following three subsections we describe experiments in which the effects of evaporative cooling and mass loading are important, discussing experimental results for a water cloud. The reference experiment with a non-evaporating oil cloud, performed to isolate the effect of mass-loading is described in the last subsection of this chapter.

Fig. 6 displays the average downward plume velocity at two measurement locations: 30 and 70 cm below the inlet. The results indicate a systematic decrease in the downdraft speed with increasing environmental humidity, demonstrating the bulk effect of evaporative cooling. The plume velocity at the inlet is 0.17 m/s. The velocities at 30 and 70 cm from the inlet indicate that the plume as a whole accelerates for the first 30 cm and then slows down. The initial acceleration is due to negative buoyancy resulting from mass loading. Lateral entrainment results both in evaporative cooling, which accelerates the plume downwards, and in a dilution of plume momentum, which decelerates the plume. The latter effect appears to prevail beyond 30 cm.

3.3. Small-scale turbulence

All of the statistical properties of velocity fluctuations analyzed below (Table 1) were obtained from the velocity retrievals described in Section 2.2. and are for cloudy filaments only. However, the analysis of small-scale velocity fluctuations from the numerical simulations of [18,19] indicates that velocity fluctuations in clear air filaments intertwined with cloud filaments are similar. The Taylor microscales in the horizontal and vertical directions are calculated from the:

$$\lambda_u^2 = \frac{\langle u'^2 \rangle}{\left\langle \left(\frac{\partial u'}{\partial x} \right)^2 \right\rangle}, \qquad \lambda_w^2 = \frac{\langle w'^2 \rangle}{\left\langle \left(\frac{\partial w'}{\partial z} \right)^2 \right\rangle}, \tag{2}$$

where u' and w' are the horizontal and vertical turbulent velocity fluctuations in the plane of the image ($u' = u - \langle u \rangle$, $w' = w - \langle w \rangle$, with u and w being the horizontal and vertical velocities); x and z are the horizontal and vertical coordinates in the image; and $\langle\rangle$ refers to an average over the image area and over many scenes.

The resulting mean Taylor microscales are $\lambda_u = 7.5 \pm 0.4$ mm and $\lambda_w = 9.2 \pm 0.6$ mm, respectively, as previously reported in [9]. For all of the experimental series λ_w/λ_u varied in the range of 1.2 to 1.5, indicating small-scale anisotropy of the flow with a preferred vertical direction (cf. Table 1). The Taylor microscale Reynolds number, Re_λ characteristic for all the experiments is obtained from:

$$Re_\lambda = \frac{TKE}{\nu} \left(\frac{10}{\Omega} \right)^{0.5}, \tag{3}$$

$$TKE = \frac{1}{2} \left(\langle u' \rangle^2 + \langle v' \rangle^2 + \langle w' \rangle^2 \right) \cong \frac{1}{2} \left(2\langle u' \rangle^2 + \langle w' \rangle^2 \right). \tag{4}$$

In (3) ν is the kinematic viscosity of the air and Ω represents the mean enstrophy of the flow as estimated from:

$$\Omega = \frac{1}{2} \langle |\vec{\omega}|^2 \rangle \cong \frac{3}{2} \langle \omega_y^2 \rangle, \tag{5}$$

where ω_y indicates the vorticity component perpendicular to the plane of the light sheet. The resulting value of $Re_\lambda \approx 40$ is substantially smaller than in natural clouds. Siebert et al. [4] report $Re_\lambda \approx 5 \cdot 10^3$ in the topmost region of stratocumulus clouds.

The *TKE* dissipation rate was estimated assuming statistical invariance in horizontal plane:

$$\varepsilon = \nu \left\langle 2 \left(\frac{\partial u}{\partial x} \right)^2 + 4 \left(\frac{\partial u}{\partial z} \right)^2 + 2 \left(\frac{\partial w}{\partial x} \right)^2 + \left(\frac{\partial w}{\partial z} \right)^2 \right\rangle. \tag{6}$$

ε varies in course of the measurements from 5×10^{-3} m^2/s^3 to 2.3×10^{-2} m^2/s^3 (cf. Table 1), which is significantly higher than that reported in [4], with a value of $\varepsilon = 2.83 \times 10^{-4}$ m^2/s^3, but is in a range of values typical for vigorous cumulus clouds [24]. These estimates indicate that the turbulence in the plume is much less developed and less intermittent than that in natural clouds and is more vigorous than that in the majority of warm clouds.

Of particular interest is the dependence of the small-scale turbulence (estimated by the ε) on the *RH* of the environment and on the distance from the inlet to the chamber, as shown in Fig. 7. At all distances, a high *TKE* dissipation rate ε corresponds to a low environmental *RH*. An increase of *RH* from 20% to 60% correlates with a systematic decrease in ε. This correlation supports the claim that small-scale velocity fluctuations result from fluctuations in the buoyancy caused by evaporative cooling at the cloud-clear air interfaces.

Please cite this article in press as: P.M. Korczyk, et al., Turbulent mixing of clouds with the environment: Small scale two phase evaporating flow investigated in a laboratory by particle image velocimetry, Physica D (2011), doi:10.1016/j.physd.2011.11.003

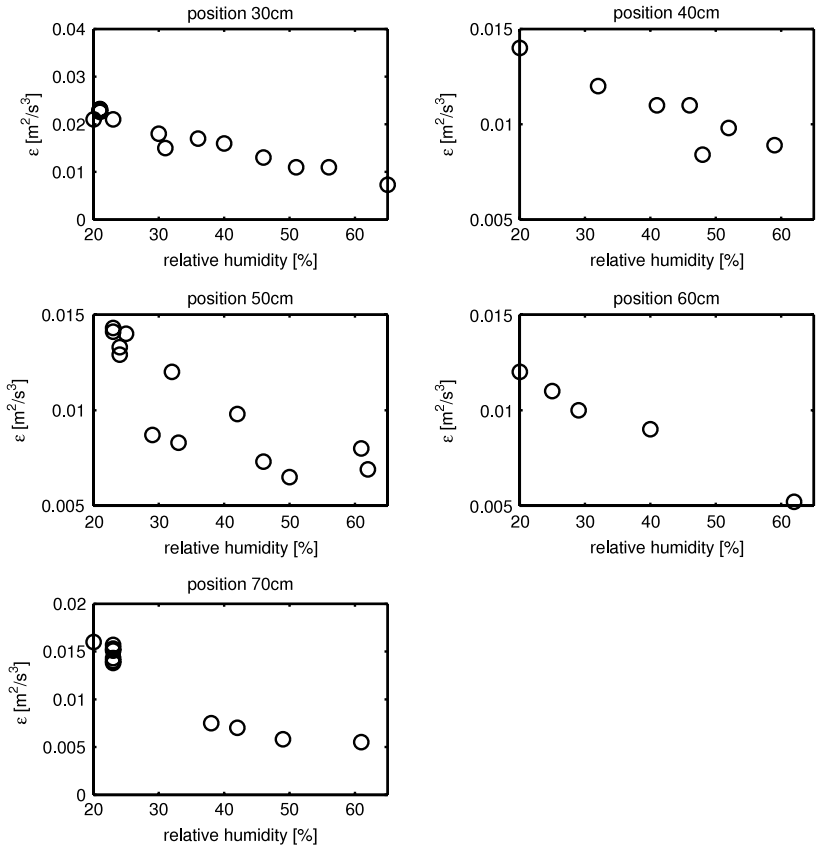

Fig. 7. Dependence of the *TKE* dissipation tare on the relative humidity in the cloud chamber. Consecutive plots show results of measurements at 30, 40, 50, 60 and 70 cm from the inlet to the cloud chamber.

The maximum values of ε are found at a distance of 30 cm from the outlet, which is consistent with the maximum downward velocity of the plume at this location. For a low environmental *RH*, there is no systematic decrease of ε with distance, suggesting that, even 70 cm from the inlet, small-scale turbulence is still actively produced by buoyancy fluctuations.

The experimental probability distribution functions (PDFs) of the velocity fluctuations in the horizontal (u') and vertical (w') directions were previously discussed in [22]. The moments of (u') and (w') collected in Table 1 demonstrate that the PDF's are close to Gaussian. In each measurement series the PDF of w' is wider than the PDF of u'. The ratio of the velocity variances $\langle w'^2\rangle/\langle u'^2\rangle = 1.74\pm0.3$ (averaged over all 50 experiments, Table 2) is consistent with the numerical simulations of Andrejczuk et al. [18,19].

3.4. Autocorrelations and structure functions

More information regarding the anisotropy can be inferred from the second-order structure functions of the turbulent velocity fluctuations, calculated according to the following formulas:

$$\begin{aligned} S_u^{\parallel}(l) &= \langle[u'(x+l,z)-u'(x,z)]^2\rangle,\\ S_w^{\parallel}(l) &= \langle[w'(x,z+l)-w'(x,z)]^2\rangle,\\ S_u^{\perp}(l) &= \langle[u'(x,z+l)-u'(x,z)]^2\rangle,\\ S_w^{\perp}(l) &= \langle[w'(x+l,z)-w'(x,z)]^2\rangle. \end{aligned} \tag{7}$$

In the above equations, the superscripts $\parallel$ and $\perp$ denote directions longitudinal and transversal to the velocity component in the subscript.

Fig. 8(a) and (b) shows the structure functions from the first measurement series (at a distance 70 cm from the orifice plotted in the log–log coordinates). The figure indicates that the measurements resolve the dissipation range of the flow (slope l^2 at scales less than ∼0.2 mm) and the smallest scales of turbulence (slope $l^{2/3}$ at scales above 1 mm). The estimate of the Kolmogorov microscale (∼0.8 mm, Table 1) is in concordance with the region of slope change. The anisotropy of the flow, as revealed by the difference in values of the structure functions of the horizontal and vertical velocity fluctuations, is even more pronounced on plots showing the autocorrelations R of u' and w' (Fig. 8(c) and (d)):

$$\begin{aligned} R_u^{\parallel}(l) &= \langle u'(x+l,z)\cdot u'(x,z)\rangle,\\ R_w^{\parallel}(l) &= \langle w'(x,z+l)\cdot w'(x,z)\rangle,\\ R_u^{\perp}(l) &= \langle u'(x,z+l)\cdot u'(x,z)\rangle,\\ R_w^{\perp}(l) &= \langle w'(x+l,z)\cdot w'(x,z)\rangle. \end{aligned} \tag{8}$$

The vertical velocity fluctuations are positively correlated for distances l exceeding 5 cm in the vertical direction, whereas correlations in horizontal direction drop to 0 on 2.5 cm distance. The horizontal velocity fluctuations decorrelate at 2.5 cm in the horizontal direction and at 3.5 cm in the vertical direction.

A comparison of structure functions from the same location (30 cm below outlet) for various environmental *RH* values (Fig. 9, linear coordinates) indicates a monotonic increase in the velocity variance with decreasing humidity. The structure function shows that the velocity differences increase rapidly at distances of 1–2 cm. For greater distances, the velocity differences grow more gradually. The position of the bending point distinguishing the rapid and gradual increase of structure function, moves from 1 to 2 cm as the environmental *RH* increases. The absolute values of the structure functions grow with the decreasing environmental *RH* which clearly indicates the role of evaporative cooling and related production of buoyancy. This inference is corroborated by the plots in Fig. 10 illustrating changes in the second order structure

Please cite this article in press as: P.M. Korczyk, et al., Turbulent mixing of clouds with the environment: Small scale two phase evaporating flow investigated in a laboratory by particle image velocimetry, Physica D (2011), doi:10.1016/j.physd.2011.11.003

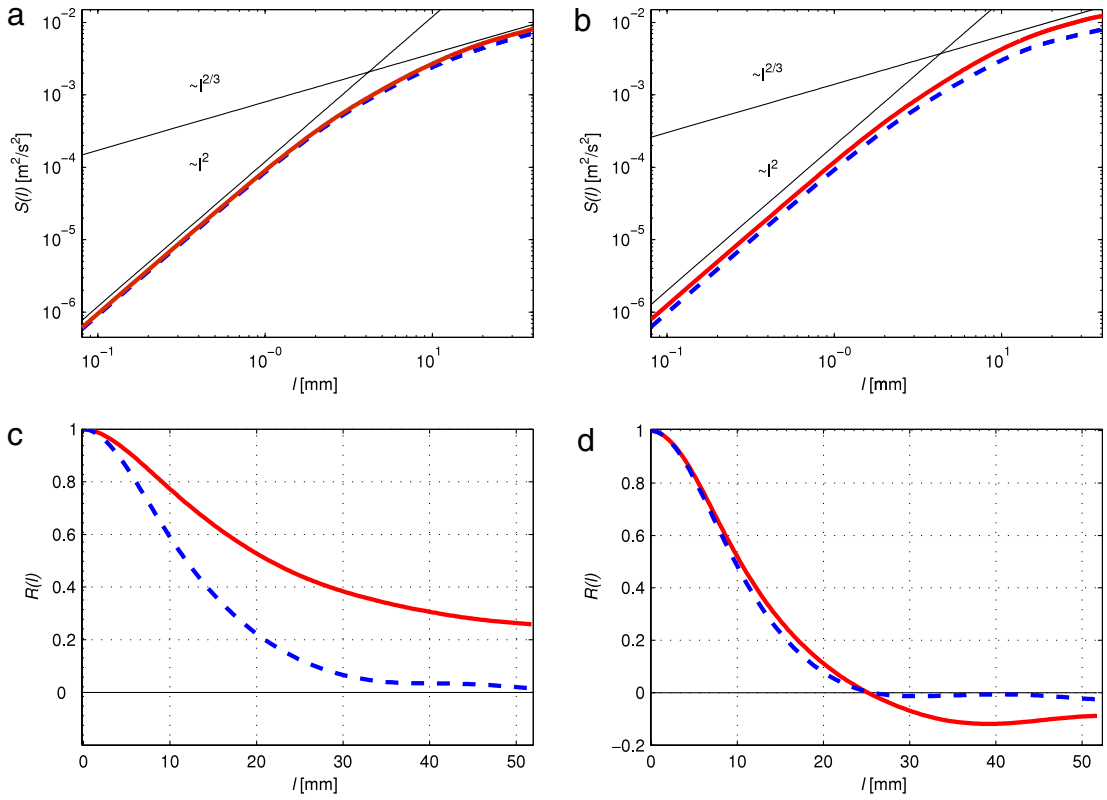

Fig. 8. Second-order structure functions and autocorrelations of velocity fluctuations at a distance of 70 cm from the orifice. (a) Longitudinal structure function, (b) transversal structure function, (c) longitudinal autocorrelation, d) transversal autocorrelation. Functions and autocorrelations calculated for both components of the velocity field: dashed line—horizontal velocity component (u); solid line—vertical velocity component (w). Note that the correlations were normalized to the product of the standard deviations of the velocity fields.

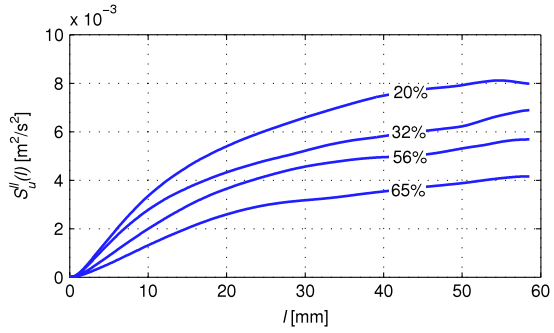

Fig. 9. Longitudinal second-order structure function of u for varying relative humidities of the environmental air, measured 30 cm from the inlet.

functions for the distance from the plume inlet at low *RH* (∼20%). It should be noted that $S_w^{\perp}$ reaches values twice as large as all of the other structure functions, indicating that the vertical direction is preferred.

At distances 50 and 70 cm from the inlet $S_w^{\parallel}$ does not change much, while $S_w^{\perp}$ decreases as a function of distance from the inlet (Fig. 10). Both $S_u^{\perp}$ and $S_u^{\parallel}$ do not change much, except for less pronounced bending at $l \approx$ 1–2 cm. This anisotropy clearly demonstrates the role of vertical motion due to buoyancy fluctuations which add energy to scales of motion close to the dissipation range.

3.5. Reference measurement

To better understand the effect of evaporative cooling of droplets, additional measurements with a plume of non-evaporating droplets were collected. A cloud was formed from a mist of DEHS (Di-Ethyl-Hexyl-Sebacat, $C_{26}H_{50}O_4$) oil. Its density is almost the same as water (912 g/l), and the droplets in the plume had a similar mean droplet diameter. Unfortunately, the mass loading (∼8 g/m^3) was lower relative to the moist plume, and we were unable to reconstruct similar dynamical conditions at the inlet. Even with some dynamical forcing turbulence was less vigorous than that of the water plume.

The velocity fluctuation results for the DEHS plume are summarized in Table 3. The table indicates that the flow decelerates more rapidly than in the evaporating case. The bulk velocities are an order of magnitude lower than those in the moist plume, and they decrease rapidly with distance from the inlet. Similarly, estimates of ε indicate a fast depletion of the *TKE*. The statistics of the velocity fluctuations indicate a preferred vertical direction, which is most likely due to the mass loading of DEHS oil in air. A striking difference in the shape of the structure functions is presented in Fig. 11. There is only a gradual increase in velocity

Table 2
Distribution of horizontal (u') and vertical (w') turbulent velocity fluctuations. Average from 50 experiments with evaporating droplets.

	Standard deviation [cm/s]	Skewness	Kurtosis
u'	5.4	−0.01	3.2
w'	8.0	−0.2	3.1

Table 3
Summary of reference measurements with non-evaporating droplets (DEHS oil).

No.	Pos. [cm]	$\langle w \rangle$ [m/s]	ε [m^2/s^3]	$\langle w'^2 \rangle / \langle u'^2 \rangle$
1	30	0.026	0.00020	1.15
2	50	0.018	0.00006	1.18
3	70	0.009	0.00001	1.17

Please cite this article in press as: P.M. Korczyk, et al., Turbulent mixing of clouds with the environment: Small scale two phase evaporating flow investigated in a laboratory by particle image velocimetry, Physica D (2011), doi:10.1016/j.physd.2011.11.003

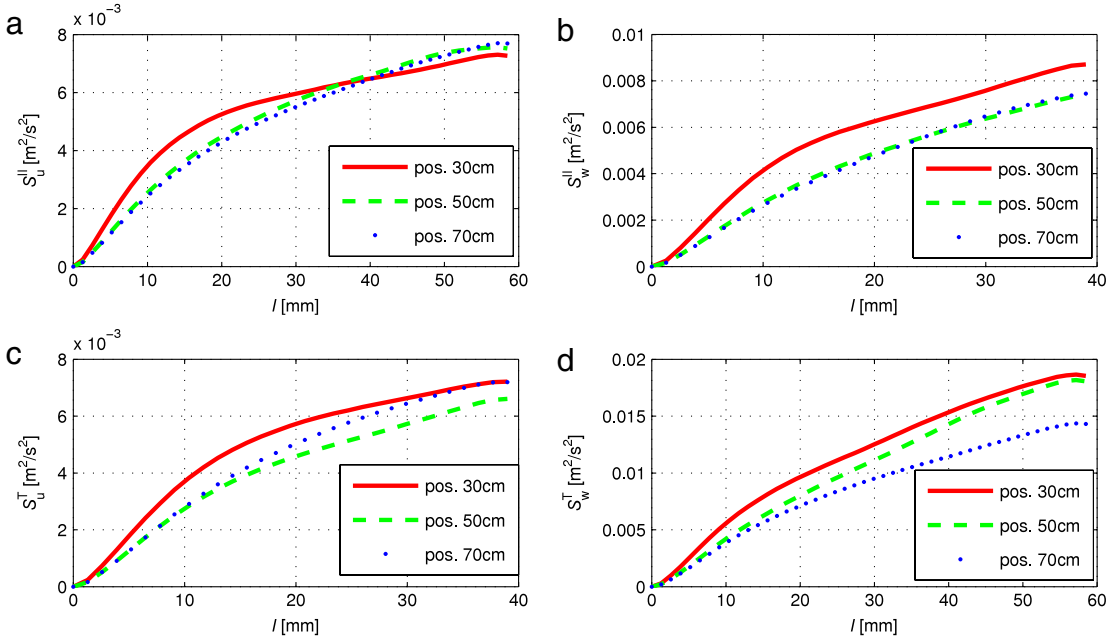

Fig. 10. Comparison of the structure functions at the various distances from the inlet, averages from measurements at low (20%–23%) *RH*'s of the environment.

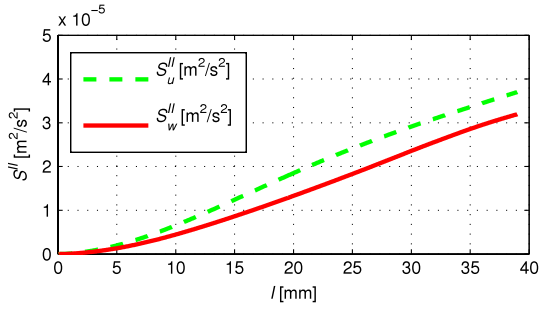

Fig. 11. Structure functions for the velocity fluctuations of the reference experiment with DEHS oil.

differences on small scales up to 2 cm, and beyond that, the structure functions bend in the direction opposite to that of the evaporating cloud.

4. Summary and conclusions

Mimicking a natural cloud a negatively buoyant saturated plume containing small droplets of water was investigated in a laboratory chamber using a PIV technique and the properties of small-scale turbulence were analyzed. The measurements were collected in such a manner as to overemphasize the effects of mass loading and evaporative cooling relative to the conditions expected in natural clouds. Under such conditions, buoyancy fluctuations resulting both from uneven evaporative cooling at the edges of filaments created in the course of mixing and from uneven mass loading produce anisotropic small-scale turbulence with a preferred vertical direction.

The effect of mass loading is straightforward: various densities of cloud and clear air filaments influence the small-scale turbulent motions caused by their differential buoyancy. The anisotropy of the small-scale turbulence was noticeable in the experiment with non-evaporating DEHS oil, for which no evaporative cooling was present.

The effect of evaporative cooling of water droplets depends on the thermodynamic properties of the cloud and of clear air. The mixing diagram in Fig. 5 shows the possible range of buoyancy fluctuations due to mass loading and evaporative cooling together. The increased range of buoyancy fluctuations due to increased effects of evaporative cooling under certain conditions (low environmental *RH*) results in more intense turbulence.

Substantial differences in the shape of the second-order structure functions of the velocity fluctuations between the evaporative and non-evaporative cases were shown in Figs. 9–11. The variance in the velocity fluctuations grows rapidly over short distances in an evaporating plume relative to a non-evaporating plume; this distinction is the result of differences in the small-scale turbulence for the two cases. The rapid growth of the small-scale velocity differences below 2 cm can be attributed to buoyancy fluctuations in a narrow sheet at the cloud-clear interface, which produces small-scale *TKE*. This phenomenon affects the typical situation of turbulence cascade, with the end of the spectrum being mostly affected by viscous dissipation. Buoyancy fluctuations at the interface result from evaporative cooling of cloud droplets close to the interface. This effect adds additional energy to the small-scale turbulence, which manifests as an increased variance of the velocity fluctuations. In particular, the fact that $S_w^{\perp}$ has substantially larger values than the other structure functions indicates that buoyancy fluctuations produce small-scale updrafts and downdrafts.

Because a fixed spectrum of droplet size distribution was used in the experiment, we were unable to address the transport of liquid water due to the sedimentation of droplets across the interface between cloudy and clear filaments, which influences the evaporation buoyancy production, as shown in numerical simulations [19,20]. One may hypothesize that all of the factors influencing the velocities and accelerations of droplets in turbulence, even caustics (the sling effect, see e.g. [29]) may also influence transport of liquid water from saturated to unsaturated filaments and hence the evaporation rate and thickness of sheets with buoyancy fluctuations. This hypothesis should be verified by further experiments with particle tracking and by particle-resolving numerical simulations accounting for phase changes. However, the most important conclusion from the present experiment is that in the two-phase evaporating flow the buoyancy production due to the evaporative cooling of small drops may measurably affect the small-scale statistics of turbulence. This result cannot be extended to clouds in natural conditions in a

Please cite this article in press as: P.M. Korczyk, et al., Turbulent mixing of clouds with the environment: Small scale two phase evaporating flow investigated in a laboratory by particle image velocimetry, Physica D (2011), doi:10.1016/j.physd.2011.11.003

straightforward manner due to an unrealistically high mass loading, a much smaller Re_λ and overemphasized evaporative cooling as compared to the conditions expected in natural clouds. The turbulence measurements for stratocumulus and shallow cumulus clouds reported in [7] with resolution of $\sim$10 cm do not indicate anisotropy. However, in such clouds, with a *LWC* almost two orders of magnitude smaller than in the experiment, effects of evaporative cooling and mass loading were weak. These effects grow with increasing liquid water content in clouds and decreasing environmental humidity. The numerical simulations of [18–20], in which the thermodynamic conditions were close to those in some cumulus clouds, indicate that in-situ measurements in preferable conditions should be performed to investigate importance of anisotropy and enhancement of small-scale turbulence present in the nature due to the evaporative cooling at the cloud-clear air interface.

Acknowledgments

This work was partly supported by Ministry of Science and Education grant No. PBZ-MNiSW-DBO-03/I/2007. SPM acknowledges International Collaboration for Turbulence Research.

References

[1] K.R. Sreenivasan, R.A. Antonia, The phenomenology of small-scale turbulence, Annu. Rev. Fluid Mech. 29 (1997) 435–472.
[2] Z. Warhaft, Passive scalars in turbulent flows, Annu. Rev. Fluid Mech. 32 (2000) 203–240.
[3] P.E. Dimotakis, Turbulent mixing, Annu. Rev. Fluid Mech. 37 (1) (2005) 329–356.
[4] H. Siebert, R.A. Shaw, Z. Warhaft, Statistics of small-scale velocity fluctuations and internal intermittency in marine stratocumulus clouds, J. Atmospheric Sci. 67 (2010) 262.
[5] J. Heintzenberg, R.J. Charlson, Clouds in the Perturbed Climate System, Mit Press, 2009.
[6] E. Bodenschatz, S.P. Malinowski, R.A. Shaw, F. Stratmann, Can we understand clouds without turbulence? Science 327 (5968) (2010) 970–971.
[7] H. Siebert, K. Lehmann, M. Wendisch, Observations of small-scale turbulence and energy dissipation rates in the cloudy boundary layer, J. Atmospheric Sci. 63 (5) (2006) 1451.
[8] H. Stommel, Entrainment of air into a cumulus cloud, J. Meteorol. 4 (3) (1947) 91–94.
[9] J. Starr Malkus, On the formation and structure of downdrafts in cumulus clouds, J. Meteorol. 12 (4) (1955) 350–354.
[10] J.W. Telford, J. Warner, On the measurement from an aircraft of buoyancy and vertical air velocity in cloud, J. Atmospheric Sci. 19 (5) (1962) 415–423.
[11] I.R. Paluch, The entrainment mechanism in colorado cumuli, J. Atmospheric Sci. 36 (12) (1979) 2467–2478.
[12] J.W. Deardorff, Cloud top entrainment instability, J. Atmospheric Sci. 37 (1) (1980) 131–147.
[13] D.A. Randall, Conditional instability of the first kind upside-down, J. Atmospheric Sci. 37 (1) (1980) 125–130.
[14] J. Mellado, B. Stevens, H. Schmidt, N. Peters, Buoyancy reversal in cloud-top mixing layers, Q. J. R. Meteorol. Soc. 135 (641) (2009) 963–978.
[15] J. Mellado, The evaporatively driven cloud-top mixing layer, J. Fluid Mech. 660 (2010) 5–36.
[16] O. Pauluis, J. Schumacher, Idealized moist Rayleigh–Bénard convection with piecewise linear equation of state, Commun. Math. Sci. 8 (2010) 295–319.
[17] S.P. Malinowski, I. Zawadzki, P. Banat, Laboratory observations of cloud-clear air mixing at small scales, J. Atmos. Ocean. Technol. 15 (4) (1998) 1060–1065.
[18] M. Andrejczuk, W.W. Grabowski, S.P. Malinowski, P.K. Smolarkiewicz, Numerical simulation of cloud-clear air interfacial mixing, J. Atmospheric Sci. 61 (14) (2004) 1726–1739.
[19] M. Andrejczuk, W.W. Grabowski, S.P. Malinowski, P.K. Smolarkiewicz, Numerical simulation of cloud-clear air interfacial mixing: effects on cloud microphysics, J. Atmospheric Sci. 63 (12) (2006) 3204–3225.
[20] M. Andrejczuk, W.W. Grabowski, S.P. Malinowski, P.K. Smolarkiewicz, Numerical simulation of cloud-clear air interfacial mixing: homogeneous versus inhomogeneous mixing, J. Atmospheric Sci. 66 (8) (2009) 2493–2500.
[21] P. Korczyk, S.P. Malinowski, T.A. Kowalewski, Mixing of cloud and clear air in centimeter scales observed in laboratory by means of particle image velocimetry, Atmos. Res. 82 (1–2) (2006) 173–182.
[22] S.P. Malinowski, M. Andrejczuk, W.W. Grabowski, P. Korczyk, T.A. Kowalewski, P.K. Smolarkiewicz, Laboratory and modeling studies of cloud-clear air interfacial mixing: anisotropy of small-scale turbulence due to evaporative cooling, New J. Phys. 10 (7) (2008) 075020.
[23] M. Raffel, C.E. Willert, J. Kompenhans, Particle Image Velocimetry: A Practical Guide, Springer, ISBN: 3-540-63683-8, 1998.
[24] H.R. Pruppacher, J.D. Klett, Microphysics of Clouds and Precipitation, Springer, 1996.
[25] P.M. Korczyk, Effect of cloud water on small-scale turbulence—laboratory model, Ph.D. Thesis, IPPT, Polish Academy of Sciences, 2008 (in Polish). Available at: http://prace.ippt.gov.pl/IFTR_Reports_4_2008.pdf.
[26] F. Toschi, E. Bodenschatz, Lagrangian properties of particles in turbulence, Annu. Rev. Fluid Mech. 41 (2009) 375–404.
[27] K.A. Emanuel, Atmospheric Convection, Oxford University Press, 1994.
[28] W. Grabowski, Cumulus entrainment, fine-scale mixing, and buoyancy reversal, Q. J. R. Meteorol. Soc. 119 (513) (1993) 935–956.
[29] G. Falkovich, A. Pumir, Sling effect in collisions of water droplets in turbulent clouds, J. Atmospheric Sci. 64 (12) (2007) 4497–4505.

Please cite this article in press as: P.M. Korczyk, et al., Turbulent mixing of clouds with the environment: Small scale two phase evaporating flow investigated in a laboratory by particle image velocimetry, Physica D (2011), doi:10.1016/j.physd.2011.11.003